RSC Advances

ROYAL SOCIETY OF CHEMISTRY

www.rsc.org/advances

Journal Name

RSCPublishing

ARTICLE

Enhanced capacitive desalination of MnO_2 by forming composite with multi-walled carbon nanotubes

Cite this: DOI: 10.1039/x0xx00000x

Received 00th January 2012,
Accepted 00th January 2012

DOI: 10.1039/x0xx00000x

www.rsc.org/

Binwei Chen,[a] Yanfang Wang,[a] Zheng Chang,[a] Xiaowei Wang,[a] Minxia Li,[a] Xiang Liu,[b*] Lixin Zhang[a],*, and Yuping Wu[a,b,*]

The morphology and structure of the prepared MnO_2/MWCNTs (multi-walled carbon nanotubes) composite are characterized by XRD, SEM, TEM, and N_2 sorption analysis. The electrochemical performance of the composite is studied by cyclic voltammetry, electrochemical impedance spectroscopy, and galvanostatic charge/discharge evaluation. The composite has a specific capacitance of 144 F g^{-1} at the current density of 1 A g^{-1}. It has higher conductivity which is affirmed by electrochemical impedance spectroscopy (EIS). The capacitive deionization (CDI) test was conducted in a bath mode apparatus by assembling a capacitor. The capacitor made from MnO_2/MWCNTs composite shows a higher desalination capacity of (6.65 mg g^{-1}) in NaCl aqueous solution, higher than that made from the virginal MnO_2 (1.60 mg g^{-1}) and those of the formerly reported. Furthermore, the MnO_2/MWCNTs composite electrode shows excellent recyclability with an efficient and rapid regeneration process.

Introduction

Nowadays, due to the population expansion and the increased agricultural activities, many countries over the world are suffering from a shortage of fresh water, which has considerably affected the environment, energy, food, economy and the living standards of people.[1] In terms of increasing water supply and managing water demand, seawater desalination is a key technology to enhance both the quantity and quality of water.[2] Conventional desalination technologies include multi-effect distillation[3] (MED), multi-stage flash[4] (MSF), reverse osmosis[5] (RO), nuclear desalination[6] and electrodialysis[7] (ED) technologies. However, these desalination technologies have some problems such as secondary pollution, high cost, maintenance difficulty, and high energy consumption.[8] Capacitive desalination technology is new technology which is based on a capacitor and characteristic by low cost and low energy consumption. Specifically, when an external direct voltage (<2 V) is imposed on the electrodes, an electrochemical double layer would be formed in the solution-electrode interface for holding ions. Once the external power is removed or even reversed, the adsorbed ions would be released back to solution resulting in the regeneration.[9]

Basically, the desalination capacity of capacitive deionization (CDI) is mainly governed by the electrode materials. The electrode should has high specific surface area for absorbing ions, good electrical conductivity for decreasing the contact resistance, appropriate pore size, and stable structure for smooth movement of ions and electrolyte wetting[10]. Carbon materials such as carbon aerogels,[11-13] activated carbon (AC),[14-18] graphene,[19-21] ordered mesoporous carbon (OMC),[22-25] hollow carbon nanofibers,[26] and carbon nanotubes (CNTs)[27-29] could meet the requirements of CDI electrodes. MnO_2 has more advantages among the transition metal oxides such as eco-friendly, low price, good chemical stability and high capacitance, and is widely used in other applications such as supercapacitors and lithium-ion battery.[30-34] However, the major drawbacks of MnO_2 include its poor electrical conductivity and low specific surface area, which impair their desalination performance. In order to overcome these limitations, an effective approach is to introduce the electronically conductive materials such as CNTs including single-walled carbon nanotubes (SWCNTs) and multi-walled carbon nanotubes (MWCNTs), which are considered as potential electrode materials for CDI due to their large intrinsic

[a] New Energy and Materials Laboratory (NEML), Department of Chemistry & Shanghai Key Laboratory of Molecular Catalysis and Innovative Materials, Fudan University, Shanghai 200433, China. E-mail: wuyp@fudan.edu.cn; Fax: +86-21-55664223
[b] College of Energy, Nanjing Tech University, Nanjing 211816, Jiangsu Province, China

area, good electrical conductivity and chemical stability.[35]

There are some researches in this area of coating MnO_2 on CNTs. A simple chemical bath mode method has been applied to synthesize MnO_2/CNT composites, which could achieve 250 F g^{-1} at 1 A g^{-1}.[36] More interestingly, a chemical vapor deposition method can be used to grow CNTs on the stainless steel meshes and then the synthesized MnO_2 via a cathodic deposition.[37] Furthermore, a three-dimensional MnO_2/CNTs composite was prepared by a facile hydrothermal method.[38]

However, there are few reports on MnO_2/CNTs composites for CDI technology. In this paper, we synthesized MnO_2/MWCNTs composite and used them as electrode materials for a capacitor in desalination experiment. Results show that the MnO_2/MWCNTs composite shows a desalination capacity of 6.65 mg g^{-1} in 30 mg L^{-1} NaCl aqueous solution, much higher than those made from the virginal MnO_2 (1.60 mg g^{-1}) and the other reported values. In addition, it can meet many CDI electrode requirements such as high desalination efficiency, low cost, and environmental friendly, which provides great promise for practical application of CDI technology.

Experimental

Preparation of composite: The MWCNTs were purchased from Chengdu Organic Chemicals Co. Ltd., Chinese Academy of Science. The activated carbon was purchased from Ningde Xinseng chemical and Industrial Co., Ltd., and used as received, which has a specific surface area of about 1600 m^2/g. All other chemical reagents in this work were of analytical grade purity from Sinopharm Chemical Reagent Co. Ltd, and used without any purification, and deionized water was used throughout the process. MnO_2 was deposited on MWCNTs through a direct redox reaction. Firstly, the MWCNTs with the diameter of 30-50 nm was dispersed in 6 M HNO_3 for 1 h with sonication and stirring for another 1 h to remove the impure substances and endow the surface with hydrophilic groups such as -OH and –COOH.[39] Then, 200 mg of the acid treated MWCNTs was immersed into an aqueous solution of 100 mL 0.1 M $KMnO_4$ and 100 mL 0.2 M H_2SO_4 at 85 °C for 1 h. Finally, the mixture was thoroughly filtered with deionization water. The product was dried at 80 °C overnight to obtain MnO_2/MWCNTs composite. For comparison, δ-MnO_2 was synthesized by using a simple solution method which was shown in Supporting Information (SI).

Characterization: The crystal structures of the samples were characterized using a Bruker D4 X-ray diffractometer with Cu K_α radiation (λ = 1.54056 Å) over a range of 2θ angles from 10° to 90°. The scanning electron microscopic (SEM) measurements were carried out using a Philip XL 300 microscope. A JEOL JEM-2010 transmission electron microscope (TEM) was used to characterize the microstructure of the MnO_2/MWCNTs composite. Elemental composition of the composite was measured with energy dispersive spectroscopy (EDS) microanalysis attached to the SEM instrument. Nitrogen adsorption-desorption isotherms were measured with TRISTAR3000, MICROMERITICS. Specific surface areas were calculated by Brunauer-Emmett-Teller (BET) method. The Barrett–Joyner–Halenda (BJH) model was used to calculate the pore size distributions curve. The thermal behavior of the composite was characterized by the thermal analysis (TG) and differential scanning calorimeter (DSC) analysis (TGA, Du-Pont TGA-2950) at a rising rate of 10°C min^{-1} from room temperature to 800 °C in the air atmosphere.

Electrochemical tests: The working electrode was prepared by mixing 75 wt.% active material, 20 wt.% acetylene black and 5 wt.% PTFE with the help of some ethanol. Then the mixture was coated onto a stainless steel mesh. After coating, the electrodes were dried at 80°C overnight. The electrochemical measurements were conducted in a three-electrode electrochemical cell connected to an electrochemical working station of CHI440B at room temperature. The three compartment cell including a MnO_2/MWCNTs composite electrode, a stainless steel mesh, and a saturated calomel electrode (SCE), which were used as the working, counter and reference electrodes, respectively. Cyclic voltammetry (CV) tests were carried out in 0.5 M NaCl aqueous solution which is similar to the concentration of the sea water within the potential range from 0 to 1.0 V. The galvanostatic charge/dischage measurements were conducted using an automatic LAND battery test instrument. The charge-discharge performance was evaluated in 0.5 M NaCl aqueous solution. The specific capacitance was calculated according the following equation:

$$C_s = \frac{I\Delta t}{m\Delta V} \quad (1)$$

where C_s is the specific capacitance (F g^{-1}), I is the constant discharge current (A), Δt is the discharge time (s), m is the mass of the electrodes (g), and ΔV is the potential change during the discharge process.

Electrochemical impedance spectroscopy measurements were also measured by CHI440B. The amplitude of the perturbation was 5 mV and the data were collected in the frequency range from 0.01 Hz to 10 kHz.

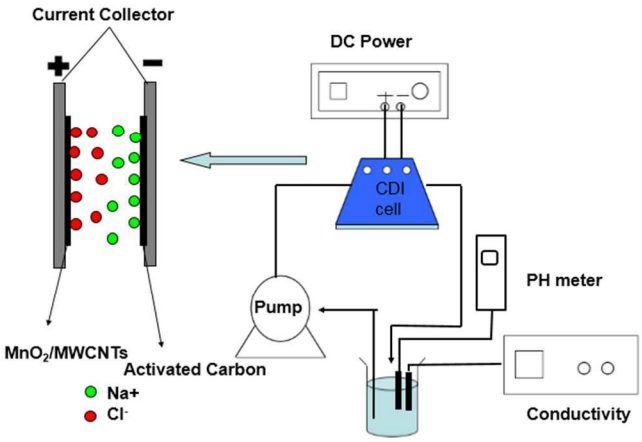

Fig.1 Schematic of the CDI system.

Desalination experiments: The CDI performance of the electrode was evaluated in a recycle system shown in Fig.1,

including a CDI cell, a peristaltic pump, a direct current power source, a conductivity meter and a pH meter. The electrodes materials were directly attached to the current collector as the CDI electrodes with a total mass of 0.2 g, the MnO_2/MWCNTs composite as the cathode and the activated carbon as the anode. In each experiment, the salty solution of 55 mL with an initial conductivity of 87 μS cm^{-1} was supplied to the CDI cell using a peristaltic pump with a flow rate of 15 mL min^{-1} and the solution temperature was kept at room temperature. Meanwhile, the amplitude of the applied voltage was 1.8 V. The regeneration of the electrodes was achieved by reversing their polarities. Here the electrosorption capacity (Q) was calculated according the following equation (2).

$$Q = \frac{(C_0 - C)V_o}{m} \qquad (2)$$

where C_0 (mg mL^{-1}) and C (mg mL^{-1}) are the initial and final concentrations, V_o (mL) is the total volume of the NaCl aqueous solution, and m (g) is the total mass of active component in the two electrodes.

Results and discussion

Morphology and structure

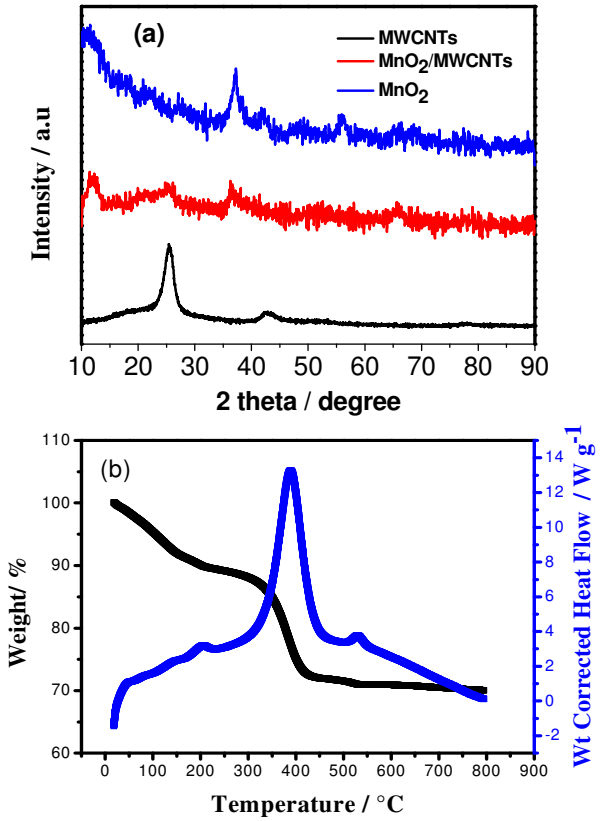

Fig. 2 (a) XRD pattern and (b) TG and DSC analysis of the MnO_2/MWCNTs composite.

The XRD pattern of the MnO_2/MWCNTs composite was shown in Fig.2a. The MWCNTs show a sharp peak at around 26° corresponding to the crystal plane of (002), and a broad weak peak at around 43° corresponding to that of (100). The MnO_2/MWCNTs composite shows another three diffraction peaks at around 12°, 37° and 67° corresponding to the crystal planes of (001), (111) and (020) for δ-MnO_2. The intensities of the MnO_2 peaks are much lower comparing with those of the peaks of the MWCNTs, indicating their poor crystallinity.

Fig.2b displays the TG and DSC analysis of the composite. The initial weight drop of ~10 wt.% below 200°C is due to the loss of the water. The following sharp decrease at about 300 °C is originated from the oxidation of MWCNTs in the air. Based on the TG analysis, the MnO_2 content is estimated to be 78 wt.% in the composite.

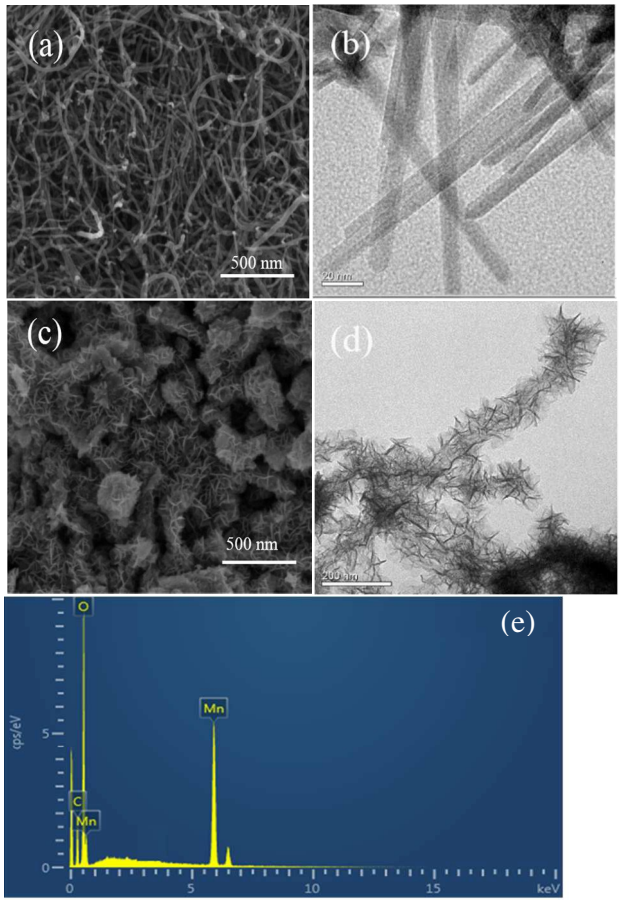

Fig.3 SEM micrographs of (a) MWCNTs, (c) MnO_2/MWCNTs composite, TEM micrograph of (b) pristine MnO_2 and (d) MnO_2/MWCNTs composite and corresponding EDX analysis (e).

As shown in Fig.3a, the acid-treated MWCNTs display that its diameter is about 30-50 nm. In Fig.3b, the MnO_2 exhibits the morphology of nanoflake. From the SEM (Fig.3c) and TEM (Fig.3d) micrographs of the composite, it can be seen that the MnO_2 is nanoflake-like (30-50 nm in thickness), and MnO_2 nanoflakes are fully grown on the surface of the MWCNTs. In addition, energy dispersive X-ray spectroscopy (EDX) analysis

in Fig.3e indicates the presence of C, Mn and O elements, which is consistent with the composite of MnO_2 with CNTs.

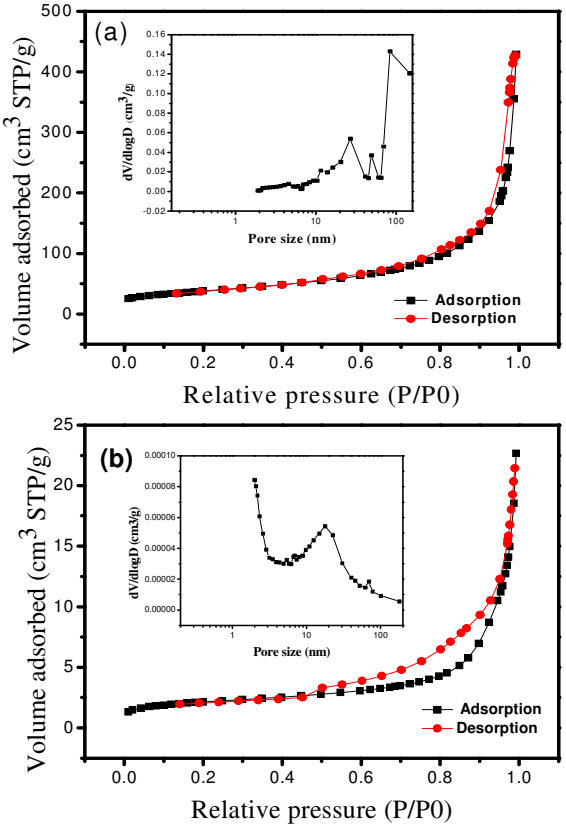

Fig.4 N_2 adsorption–desorption isotherms and pore size distribution (inset) of (a) the MnO_2/MWCNTs composite and (b) the virginal MnO_2.

Table 1 The parameters of surface area and porosity.

Sample	S_{BET} ($m^2\ g^{-1}$)	V_{tot} ($cm^3\ g^{-1}$)	D_{av} (nm)
MnO_2/MWCNTs	134	0.664	19.7
MnO_2	7.61	0.0347	18.45

The N_2 adsorption–desorption isotherms and the pore size distribution of the samples are shown in Fig.4. The parameters of the surface area and porosity were calculated and listed in Table 1. It is clearly observed that the two samples display an adsorption of Type IV with a small hysteresis loop of H3 and the pore size distribution indicates the presence of mesoporous in these porous structures. The MnO_2/MWCNTs composite displays a high specific surface area of 134 $m^2\ g^{-1}$ with a pore volume of 0.664 $cm^3\ g^{-1}$, which is much higher than the virginal MnO_2 (specific surface area of 7.61 $m^2\ g^{-1}$ and a pore volume of 0.0347 $cm^3\ g^{-1}$). This may be resulted from the addition of the MWCNTs. As to the detailed reason, it needs further investigation. The increased specific surface area and pore volume of the MnO_2/MWCNTs composite can ensure more accessible surface sites for ion adsorption during the CDI process.

Electrochemical behaviour

Fig.5a displays the CV curves of the MnO_2/MWCNTs composite and the virginal MnO_2 electrodes in 0.5 M NaCl aqueous solution at a scan rate of 1 mV s^{-1} in a potential range of 0 to 1.0 V. Both the CV curves show a nearly rectangular shape with a pair of weak redox peaks at about 0.5–0.7 V, indicating the pseudocapacitance from redox reactions between Mn(IV) and Mn(III) or Mn(II).[40] Moreover, the specific capacitance calculated according to Eqn. (1) from the CV curves is 163 F g^{-1} for the MnO_2/MWCNTs composite which is much higher than the virginal MnO_2 (119 F g^{-1}). The main reason is that the MWCNTs can not only improve the surface area of MnO_2 but also decrease the resistance of the MnO_2/MWCNTs composite.

Fig.5b shows the CV curves of the the MnO_2/WMCNTs composite in 0.5 M NaCl aqueous solution at different scan rates. It can be observed that at low scan rates, the electrode shows rectangular shape. With the increase of the scan rate, the shape of rectangle is slightly distorted due to the polarization and the resistance of the electrodes.[41] The specific capacitances of the MnO_2/MWCNTs composite are 163, 155, 144, 137, 121, 110, 93, 66 and 35 F g^{-1} at the scan rates of 1, 2, 5, 10, 20, 30, 50, 100 and 200 mV s^{-1}, respectively. Obviously, the capacitance decreases with the increase of the scan rate. This is because at high scan rate, the ions do not have enough time to diffuse into all the available pores of the MnO_2 and some internal active MnO_2 species cannot be used, which causes lower specific capacitance.[16]

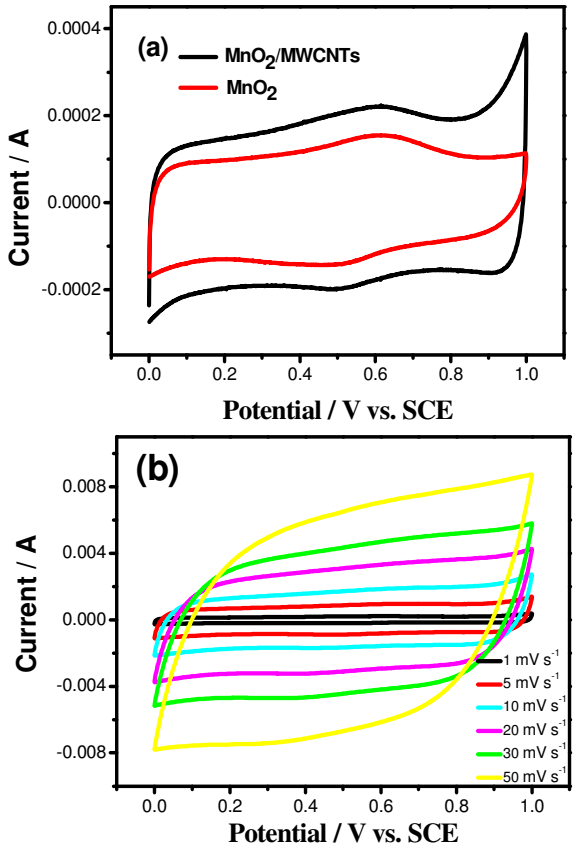

Fig. 5 CV curves for two electrodes at scan rate of 1 mV s^{-1}, (b) the MnO_2/MWCNTs composite at different scan rates in 0.5 M NaCl aqueous solution.

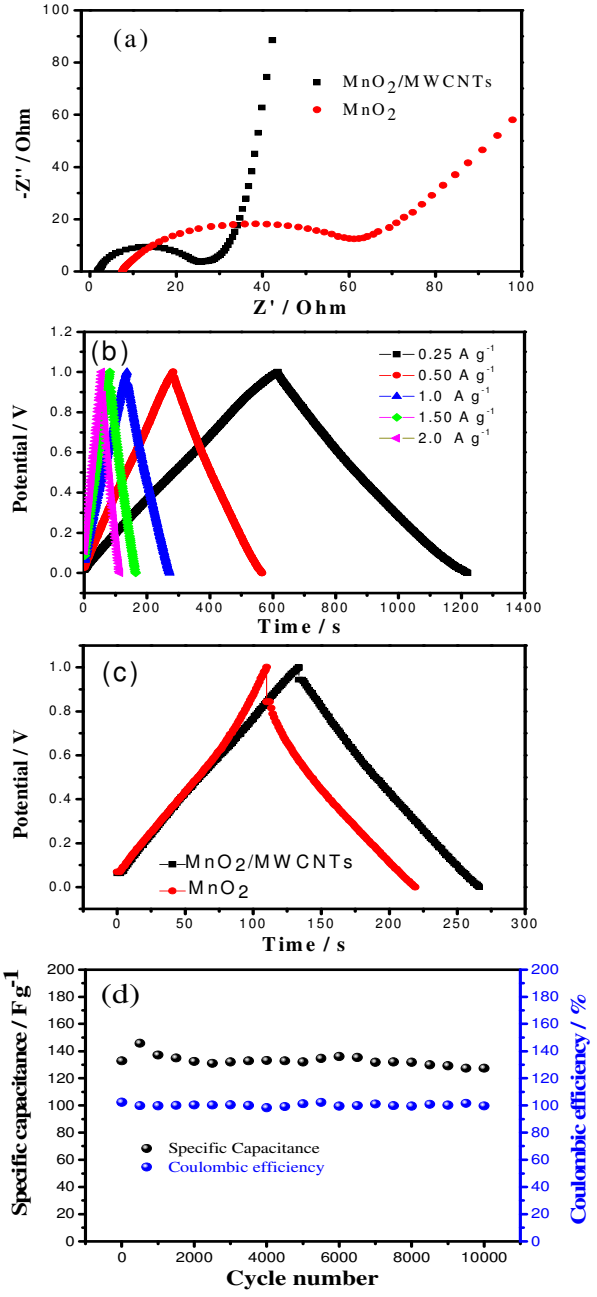

Fig.6 (a) Nyquist plots of the MnO_2 and MnO_2/MWCNTs composite electrodes in a 0.5 M NaCl aqueous solution, (b) charge/discharge curves of MnO_2/MWCNTs composite in 0.5 M NaCl aqueous solution at different current densities, (c) the charge/discharge curves of the MnO_2 and MnO_2/MWCNTs composite electrodes at the current density of 1 A g^{-1}, (d) cycling performance of the MnO_2/MWCNTs composite at 1 A g^{-1}.

The Nyquist plots for the MnO_2/MWCNTs composite and the virginal MnO_2 are shown in Fig.6a. The alternative current impedance spectra for both of them compose of a semicircle in the high-to-medium-frequency region, and a straight line at the very low-frequency region. The semicircle corresponding to a parallel combination of charge-transfer resistance (R_{ct}) and MnO_2/MWCNTs composite is smaller than that of the MnO_2, indicating that the MWCNTs can decrease the R_{ct} of the MnO_2/MWCNTs composite. The intercepts on the real Z' axis shows the equivalent series resistance (ESR) values for the electrolytes. The MnO_2/MWCNTs composite has a lower ESR value compare to the MnO_2, which refer to a lower contact resistance at the interface between the active material and the aqueous solution.[42]

Fig.6b shows the constant-current charge/discharge curve of the MnO_2/MWCNTs composite at different current density in 0.5 M NaCl aqueous solution. According to Eqn. (1), the specific capacitance of the composite is 151 F g^{-1} at low current density of 0.25 A g^{-1}. As the current density increases to 2 A g^{-1}, the specific capacitance remains at 123 F g^{-1}, less than 19% capacity fading which indicates the excellent rate capability. The charge/discharge curves of the MnO_2 and the MnO_2/MWCNTs composite in 0.5 M NaCl aqueous solution at 1 A g^{-1} is shown in Fig.6c. The discharge time of the MnO_2/MWCNTs composite electrode is longer than that of the MnO_2. The specific capacitance calculated according to Eqn. (1) is 144 F g^{-1} for the MnO_2/MWCNTs composite which is much higher than the virginal MnO_2 (109 F g^{-1}). In addition, the IR drop of the MnO_2/MWCNTs composite is smaller than that of the MnO_2 since the MnO_2/MWCNTs composite has lower internal resistance. The cycling performance of the MnO_2/MWCNTs composite at the current density of 1 A g^{-1} (Fig.6d) shows that the coulombic efficiency is almost 100 % and it loses less than 14 % of the initial capacitance after 10000 cycles. This result indicates excellent cycling stability and capacity retention in NaCl even oxygen is not removed.

CDI tests

To estimate the desalination performance of the fabricated supercapacitor, the bath mode experiments were conducted in a 30 ppm NaCl aqueous solution that has an initial conductivity of 87 μS cm^{-1} at an applied voltage of 1.8 V. Fig.7a gives the desalination curves of the cells based on the MnO_2/MWCNTs composite and the virginal MnO_2. A dramatic decrease of the conductivity appears for both cells at the beginning stage which indicates quick adsorption of the salt ions. In the second stage, the conductivity tends to get constant due to the electrosorption saturation. The electrosorption capacity of the MnO_2/MWCNTs composite cell was calculated according to Eqn. (2) as 6.65 mg g^{-1}, which is much higher than that of the cell based on the virginal MnO_2 (1.60 mg g^{-1}), and exceed those of the reports about CDI electrode materials to our knowledge, which are listed in Table 2. The superior desalination capacity of the MnO_2/MWCNTs composite is mainly due to the high specific capacitance, good conductivity, large specific surface area and suitable pore structure. Fig.7b shows the effect of applied voltage on the desalination performance. The experiments were conducted at various voltages of 1.4, 1.6, 1.8 V in 0.03 g L^{-1} NaCl solution. It can be seen that the higher the applied voltage, the higher the

desalting capacity is. When the applied voltage increases from 1.4, 1.6, to 1.8 V, the electrosorption capacity reaches 2.93, 3.87, 6.65 mg g^{-1}, respectively.

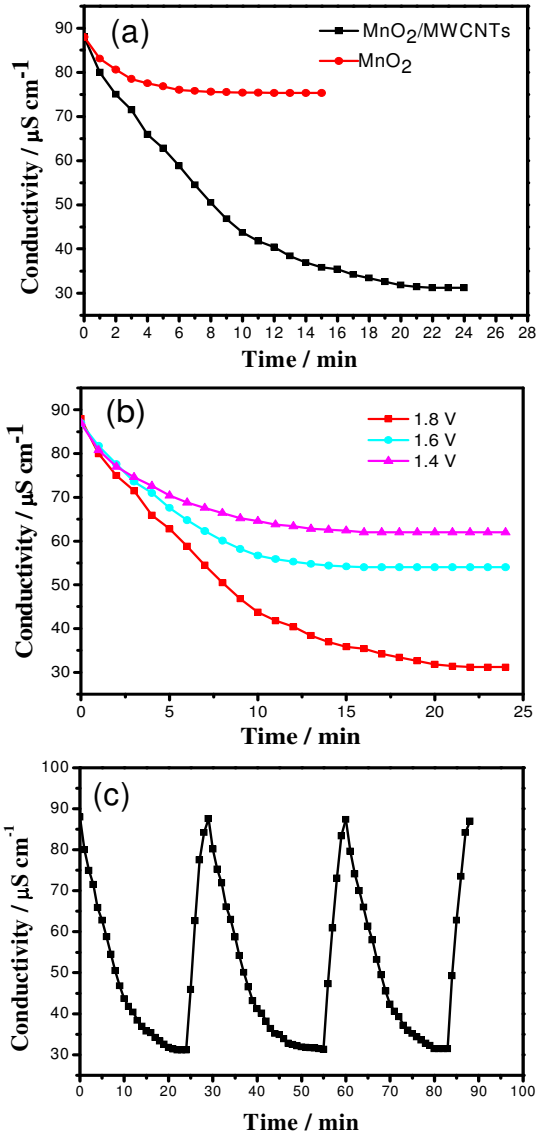

Fig.7 Desalination curves of the MnO_2/MWCNTs composite and MnO_2 (a); Electrosorption of NaCl onto MnO_2/MWCNTs composite electrode for the conductivity variation at different applied potentials (b); NaCl adsorption and regeneration curves of the composite electrodes (c)

Fig.7c displays the repeated performance of the MnO_2/MWCNTs composite electrode. The electrosorption capacity of NaCl for the cell based on the MnO_2/MWCNTs composite during the three sequent runs is 6.65, 6.59, and 6.56 mg g^{-1}, respectively. In addition, the MnO_2/MWCNTs composite electrode has no appreciable decrease in the initial conductivity. During the desalination and regeneration progress, the pH values of the solution remained stable within a range of 5.6-6.0, ensuring no hydrolysis of water.

The CDI results suggest that the MnO_2/MWCNTs composite performs very well with high desalination efficiency. Therefore, the composite has a great potential as the electrode material for CDI technology.

Table 2 Comparison of the electrosorption capacitance among different electrode materials reported in the literature.

Sample	Initial concentration (mg L^{-1})	Electrosorption capacity (mg g^{-1})	Ref.
AC	~25	0.25	43
CNTs	60	0.7	44
CNTs-MC	40	0.63	45
MnO_2/NPC	50	0.988	10
AC-MnO_2	~25	0.99	46
GNS-MnO_2	100	5.01	42
MnO_2@MWCNTs	~87	6.65	This work

Note: MC for mesoporous carbon, NPC for nanoporous carbon, and GNS for graphene nanosheet.

Conclusion

In this paper, a MnO_2/MWCNTs composite was successfully synthesized through a facile and green method, and used as a potential application as an electrode of CDI device. The MWCNTs are fully and uniformly coated with MnO_2. The N_2 sorption analysis demonstrates that the MnO_2/MWCNTs composite has a larger specific surface area as compared with the virginal MnO_2. It is noted that the surface area is a decisive factor influencing the desalination capacitance.[47] In all the electrochemical evaluation, the MnO_2/MWCNTs composite exhibits superior electrochemical properties as compared with the virginal MnO_2, which is due to the larger surface area and higher electronic conductivity. Furthermore, the desalination experiments demonstrate that the removal of ions from a NaCl aqueous solution can be successfully achieved by using the MnO_2/MWCNTs composite electrodes. The electrosorptive capacity of the MnO_2/MWCNTs composite and MnO_2 is 6.65 and 1.60 mg g^{-1}, respectively. By comparing with the virginal MnO_2 electrode, the MnO_2/MWCNTs composite electrode shows larger electrosorption capacity and good repeated performance during the CDI process. Therefore, the MnO_2/MWCNTs composite can be considered as a promising material for CDI technology.

Acknowledgement: Financial support from rom China National Distinguished Youth Scientists (NSFC No. 51425301) is greatly appreciated.

Notes and references

1 M. A. Shannon, P. W. Bohn, M. Elimelech, J. G. Georgiadis, B. J. Marin and A. M. Mayes, *Nature*, 2008, **452**, 301-310.
2 R. F. Service, *Science*, 2006, **313**, 1088-1090.
3 A. Hamidi, K. Parham, U. Atikol and A. H. Shahbaz, *Desalination*, 2015, **371**, 37-45.
4 M. M. Alhazmy, *Energy*, 2014, **76**, 1029-1035.

5 M. S. Japas, N. A. Rubinstein and A. L. R. Gómez, *Ore Geol. Rev.* 2015, **71**, 191-202.
6 A. P. Avrin, G. He and D. M. Kammen, *Desalination*, 2015, **360**, 1-7.
7 X. P. Zhu, W. H. He and B. E. Logan, *J.Membrance Sci.*, 2015, **494**, 154-160.
8 X. R. Wen, D. S. Zhang, T. T. Yan, J. P. Zhang and L. Y. Shi, *J. Mater. Chem. A*, 2013, **1**, 12334-12344.
9 Z. Wang, B. J. Dou, L. Zheng, G. N. Zhang, Z. H. Liu and Z. P. Hao, *Desalination*, 2012, **299**, 96-102.
10 J. Yang, L. Zou, H. H. Song and Z. P. Hao, *Desalination*, 2011, **276**, 199-206.
11 Y. F. Zhang, W. Fan, Y. P. Huang, C. Zhang and T. X. Liu, *RSC Adv.*, 2015, **5**, 1301-1308.
12 A. Allahbakhsh and A. R. Bahramian, 2015, **5**, 14139-14158.
13 S.-A. Wohlgemuth, T.-P. Fellinger, P. Jaker and M. Antonietti, *J. Mater. Chem. A*, 2013, **1**, 4002-4009.
14 M. Sevilla and R. Mokaya, *Energy Environ .Sci*, 2014, **7**, 1250-1280.
15 P. Cheng, S. Y. Gao, P. Y. Zang, X. F. Yang, Y. L. Bai, H. Xu, Z. H. Liu and Z. B. Lei, *Carbon*, 2015, **93**, 315-324.
16 D. B. Wang, Z. Geng, B. Li and C. M. Zhang, *Electrochim. Acta*, 2015, **173**, 377-384.
17 E. J. Lee, Y. J. Lee, J. K. Kim, M. Lee, J. Yi, J. R. Yoon , J. C. Song and I. K. Song, *Mater. Res. Bull.*, 2015, **70**, 209-214.
18 Y. Gao, L. Li, Y. M. Jin, Y. Wang, C. J. Yuan, Y. J. Wei, G. Chen, J. J. Ge and H. Y. Lu, *Appl. Energy*, 2015, **153**, 41-77.
19 S. P. Wu, R. Xu, M. J. Lu, R. Y. Ge, J. Iocozzia, C. P. Han, B. B. Jiang and Z. Q. Lin, *Adv. Energy Mater.*, 2015, **5**, 1500400(1-40).
20 X. L. Wang and G. Q. Shi, *Energy Environ .Sci*, 2015, **8**, 790-823.
21 V. Meriga, S. Valligatla, S. Sundaresan, C. Cahill, V. R. Dhanak and A. K. Chakraborty, *J. Appl. Polym. Sci.*, 2015, **42766**, 1-9.
22 Z. J. Zhu, Y. J. Hu, H. Jiang and C. Z. Li, *J. Power Sources*, 2014, **246**, 402-408.
23 J. K. Hu, M. Noked, E. Gillette, Z. Gui and S. B. Lee, *Carbon*, 2015, **93**, 903-914.
24 M. Enterría, M. F. R. Pereira, J. I. Martins and J. L. Figueiredo, *Carbon*, 2015, **95**, 72-83.
25 S. Tanaka, H. Fujimoto, J. F. M. Denayer, M. Miyamoto, Y. Oumi and Y. Miyake, *Micropor. Mesopor. Mat.*, 2015, **217**, 141-149.
26 A. G. El-Deen, N. A. M. Barakat, K. A. Khalild and H. Y. Kim, *New J. Chem.*, 2014, **38**, 198-205.
27 H. Y. Liu, H. H. Song, X. H. Chen, S. Zhang, J. S. Zhou and Z. K. Ma, *J. Power Sources*, 2015, **285**, 303-309.
28 M. Li, F. Liu, J. P. Cheng, J. Ying and X. B. Zhang, *J. Alloy Compd.*, 2015, **635**, 225-232.
29 T.-T. Lin, W.-H. Lai, Q.-F. Lü and Y. Yu, *Electrochim. Acta*, 2015, **178**, 517-524.
30 X. W. Guo, J. H. Han, L. Zhang, P. Liu, A. Hirata, L. Y. Chen, T. Fujitaa and M. W. Chen, *Nanoscale*, 2015, **7**, 15111-15116.
31 C. X. Guo, A. A. Chitre and X. M. Lu, *Phys. Chem. Chem. Phys.* , 2014, **16**, 4672-4678.
32 D. J. Wu, S. H. Xu, M. Li, C. Zhang, Y. P. Zhu, Y. W. Xu, W. W. Zhang, R. Huang, R. J. Qi, L. W. Wang and P. K. Chu, *J .Mater. Chem. A*, 2015, **3**, 16695-16707.
33 M. Huang, F. Li, F. Dong, Y. X. Zhang and L. L Zhang, *Prog. Mater. Sci.*, 2015, **74**, 51-124.
34 J. Zhang, Y. P. Luan, Z. Y. Lyu, L. J. Wang, L. L. Xu, K. Yuan, F. Pan, M. Lai, Z. L. Liu and W. Chen, *Nanoscale*, 2015, **7**, 14881-14888.
35 H. J. Wang, C. Peng, F. Peng, H. Yu and J. Yang, *Mat. Sci. Eng. B*, 2011, **176**, 1073-1078.
36 S.-B. Ma, K.-W. Nam, W.-S. Yoon, X.-Q. Yang, K.-Y. Ahn, K.-H. Oh d and K.-B. Kim, *J. Power Sources*, 2008, **178**, 483-489.
37 Y. H. Wang, H. Liu, X. L. Sunb and I. Zhitomirsky, *Scripta Mater.*, 2009, **61**, 1079-1082.
38 F. Teng, S. Santhanagopalan, Y. Wang and D. D. Meng, *J. Alloy Compd.*, 2010, **499**, 259-264.
39 W. Tang, Y. Y Hou, F. X. Wang, L. L. Liu, Y. P. Wu, and K. Zhu, *Nano Lett.*, 2013, **13**, 2036-2040.
40 Q. T. Qu, P. Zhang, B. Wang, Y. H. Chen, S. Tian, Y. P. Wu and R. Holze, *J. Phys. Chem. C*, 2009, **113**, 14020-14027.
41 J. Yan, T. Wei, Z. J. Fan, W. Z. Qian, M. L. Zhang, X. D. Shen and F. Wei, *J. Power Sources*, 2010, **195**, 3041-3045.
42 A. G. El-Deen, N. A. M. Barakat and H. Y. Kim, *Desalination*, 2014, **344**, 289-298.
43 L. Zou, L. X. Li, H. H. Song and G. Morris, *Water Res.*, 2008, **42**, 2340-2348.
44 M. Wang, Z. H. Huang, L. Wang, M.-X. Wang, F. Y. Kang and H. Q. Hou, *New J. Chem.*, 2010, **34**, 1843-1845.
45 D. S. Zhang, L. Y. Shi, J. H. Fang and K. Dai, *Mater. Lett.* , 2006, **60**, 360-363.
46 J. Yang, L. Zou, H. H. Song and Z. P. Hao, *Desalination*, 2012, **286**, 108-114.
47 M. T. Z. Myint, S. H. Al-Harthi and J. Dutta, *Desalination*, 2014, **344**, 236-242.

Graphic Abstract

Enhanced capacitive desalination of MnO_2 by forming composite with multi-walled carbon nanotubes

Binwei Chen, Yanfang Wang, Zheng Chang, Xiaowei Wang, Minxia Li, Xiang Liu, Lixin Zhang, and Yuping Wu

A supercapacitor from the MnO_2/MWCNTs composite is used for deionization. It shows a high desalination capacity of 6.65 mg g^{-1} and good efficiency. This result shows that this capacitive deionization (CDI) is of great promise for practical application.